Multifunctional Additives for NO_X Abatement in Fluidized Bed Biomass Combustion

Ulusoy, Burak; Anicic, Bozidar; Zhao, Liyan; Lin, Weigang; Lu, Bona; Wang, Wei; Dam-Johansen, Kim; Wu, Hao

Published in:
Energy and Fuels

Link to article, DOI:
10.1021/acs.energyfuels.1c01186

Publication date:
2021

Document Version
Peer reviewed version

Multifunctional additives for NO_X abatement in fluidized bed biomass combustion

Burak Ulusoy [1,2,3], Bozidar Anicic [1,2,3], Liyan Zhao [1], Weigang Lin [1,3], Bona Lu[3,4], Wei Wang [3,4], Kim Dam-Johansen [1], Hao Wu [1]*

1: Department of Chemical and Biochemical Engineering, Technical University of Denmark, Søltofts Plads 229, 2800 Kgs. Lyngby, Denmark

2: Sino-Danish Centre for Education and Research, Beijing, 100093, China

3: Sino-Danish College, University of Chinese Academy of Sciences, Beijing 100049, China

4: State Key Laboratory of Multiphase Complex Systems, Institute of Process Engineering, Chinese Academy of Sciences, Beijing 100190, China

Keywords: NO_X, fluidized bed combustion, agglomeration, biomass, additive

***Corresponding author e-mail id:** haw@kt.dtu.dk, Department of Chemical and Biochemical Engineering, Technical University of Denmark, Søltofts Plads 229, 2800 Kgs. Lyngby, Denmark

Supplemental material is available

Abstract: Two major challenges in fluid bed combustion of biomass are increased NO_X emissions and bed agglomeration. Different additives were employed to simultaneously reduce NO_X emissions and bed agglomeration from fluidized bed combustion of biomass. The base fuel was straw and the additives included CaO, kaolin, $MgCO_3$, coal fly ash, clay, $(NH_4)_2Fe(SO_4)_2$, $NH_4Fe(SO_4)_2$, $(NH_4)_2SO_4$, NH_4MgPO_4, $AlNH_4(SO_4)_2$, $(NH_4)_2HPO_4$, $(NH_4)_3[Fe(C_2O_4)_3]$, and urea. The influence of $(NH_4)_2SO_4$ particle size (<35 μm and <106 μm) and introduction method (batch addition or premixing with fuel) was additionally investigated. The most effective additives against NO_X emissions and bed agglomeration were further studied in air staged straw combustion and un-staged sunflower husk combustion. During sunflower husk combustion, the influence of ash accumulation and incipient defluidization on NO_X emissions were examined. The results show that kaolin, CaO, $MgCO_3$, $(NH_4)_2Fe(SO_4)_2$, $NH_4Fe(SO_4)_2$, $AlNH_4(SO_4)_2$, and NH_4MgPO_4 prevented defluidization during straw combustion under the investigated conditions. Of these, $AlNH_4(SO_4)_2$, and NH_4MgPO_4 reduced the fuel-N to NO conversion by 40%. The mechanism of reduction was related to the facilitation of thermal $DeNO_X$ reactions by introduction of NH_3-releasing additives. However, the NH-based additives resulted in higher emissions of N_2O. The size of $(NH_4)_2SO_4$ particles had a slight influence on the defluidization tendency and nitrogen chemistry, while no significant difference was observed between the two additive introduction methods. Air staging reduced the fuel-N to NO conversion by 40% during straw combustion. The use of NH_4MgPO_4 and $AlNH_4(SO_4)_2$ under air staged conditions increased the NO emission slightly. This was predominantly caused by the combustion of NH_3 in the secondary air jet. In the case of un-staged sunflower husk combustion, NH_4MgPO_4 and $AlNH_4(SO_4)_2$ prevented defluidization, while reducing the conversion of fuel-N to NO by 30%. During sunflower husk combustion, the accumulation of ash increased NO and decreased NH_3 concentrations above the bed. This was related to the poorer mixing as the bed approached defluidization and to the catalytic effect of ash forming elements on the oxidation of NH_3 to NO.

1 Introduction

Biomass, as a CO_2 neutral and renewable fuel, has received growing interest as an alternative to coal for heat and power production. Fluidized bed combustion is a promising technology for the utilization of biomass, as it offers high fuel flexibility and combustion efficiency.[1] However, fluidized bed combustion of biomass suffer from two major challenges, NO_X emissions and bed defluidization. The increased NO_X emissions may result from the variable and sometimes very high nitrogen content in biomass, while the high potassium content in biomass may induce bed agglomeration and, in severe cases, defluidization.

The mechanisms of these challenges have been widely studied. Due to the low temperature (800-900ºC) and presence of fuel bound nitrogen (fuel-N) in fluidized bed combustion of solid fuels, the general consensus is that thermal and prompt NO_X may be neglected; hence, the major contributor to NO is from fuel-N oxidation.[2–6] Bed agglomeration is generally caused by the interaction between the ash forming elements and bed material, leading to the formation of a molten viscous phase such as K-silicates on bed particles. This sticky molten phase increases the propensity of bed particles to stick and form agglomerates, which ultimately leads to bed defluidization.[7]

Several countermeasures have been proposed to deal with NO_X emissions and bed agglomeration. Primary measures employed for NO_X emission control in fluidized bed combustion are air staging [8,9], temperature adjustment[10], SNCR[11], lowering excess air[12], reburning (fuel staging)[13,14], flue gas recirculation[15], and fuel blending[16,17]. Hybrid systems such as SNCR and air staging[11], and reburning combined with SNCR (advanced reburning)[18,19] have also been investigated. In comparison, countermeasures against bed agglomeration include the use of alternative bed materials[7,20,21], additives [22,23], co-combustion[7,24], and biomass pre-treatment[25,26]. Techniques for overcoming these two issues normally target each area independently. Hence, alternative methods aiming at reducing both NO_X emissions and bed agglomeration have, to the knowledge of the authors, not been studied.

The objective of this study is to investigate the impact of additives on NO_X emissions and bed agglomeration during fluidized bed combustion of straw. While overall results on the influence of

additives on bed agglomeration are presented in the following sections, the focal point of this work is on the NO_X emissions. The used additives are summarized in Figure 1Figure 1 in three categories based on their hypothesized impact; anti-agglomeration, de-NO_X, and multifunctional. The influence of additive particle size and additive introduction method was additionally examined in the case of $(NH_4)_2SO_4$. Selected additives were also used in air staged straw and un-staged sunflower husk combustion. Moreover, the impact of ash accumulation on NO_X emissions was investigated during un-staged sunflower husk combustion, as the defluidization time was longer for this fuel than for straw, which allowed measurements at the initial and later stages of combustion.

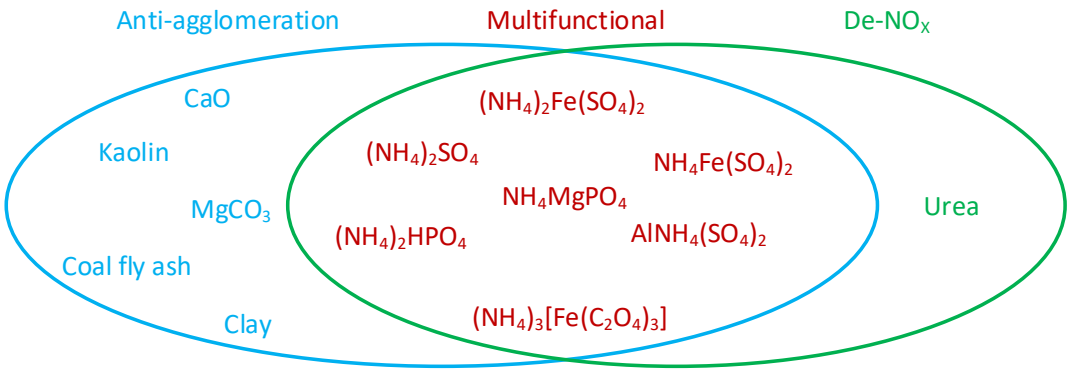

Figure 1: Illustration showing the three classes of additives employed in this study; anti-agglomeration, de-NO_X, and multifunctional.

2 Experimental

2.1 Materials

2.1.1 Fuels and bed material

Wheat straw and sunflower husk, relevant for energy production in industrial scale[27,28], were chosen as the biomass fuel, as these exhibited different Si contents and propensities for defluidization, while having a comparable amount of K. The chemical composition of the investigated biomass, wheat straw and sunflower husk, is shown in Table 1Table 1. The biomass particles were ground and sieved to a size range of 0.6-4 mm to minimize fuel particle elutriation and ensure continuous feeding. Silica sand was used as bed material in the fluidized bed (D_{50} 273 µm, 2600 kg/m^3, Geldart B).

Table 1: Fuel chemical composition

	% w.b.	% d.b.								mg/kg d.b.							
Fuel	**Moisture**	**VM**	**Ash**	**C**	**H**	**N**	**S**	**Cl**	**O**	**Al**	**Ca**	**Fe**	**K**	**Mg**	**Na**	**P**	**Si**
Wheat straw	12.5	76.5	4.6	48.7	5.8	0.69	0.08	0.18	40.0	230	3600	180	8000	630	280	750	11000
Sunfl. husk	9.1	75.8	3.2	51.7	5.7	0.80	0.14	0.04	38.4	55	3700	94	9600	2100	21	660	290

2.1.2 Additives

Thirteen additives have been were evaluated in this study. The particle size and crystalline phases of the additives are demonstrated in Table 2Table 2. Notably, Sseveral of the de-NO_X additives contained crystal water. Moreover, sSome of the additives were used as received, explaining the small differences in the employed size ranges. Generally, smaller particles were chosen to ensure adequate adhesion to the biomass particles. Two different particle sizes (<35 and <106 µm) of $(NH_4)_2SO_4$ were used. Additional information of the additives can be found in the supplemental material (Table S1).

Table 2: Particle size and crystalline phases of the additives. a: determined by XRD [29], b: determined from label.

Additive	**Particle size [µm]**	**Crystalline phases**
Kaolin [a]	< 85	$Al_2Si_2O_5(OH)_4$, SiO_2
Coal fly ash [a]	< 32	$2Al_2O_3{\cdot}SiO_2$, SiO_2
Clay [a]	< 35	$CaCO_3$, SiO_2, Al_2SiO_5
$MgCO_3$ [a]	< 25	$MgCO_3$, MgO

CaO [a]	< 50	CaO
$(NH_4)_2SO_4$ [a]	< 35 and < 106	$(NH_4)_2SO_4$
$(NH_4)_2HPO_4$ [b]	< 106	$(NH_4)_2HPO_4$
$(NH_4)_2Fe(SO_4)_2$ [b]	< 106	$(NH_4)_2Fe(SO_4)_2 \cdot 6\ H_2O$
$NH_4Fe(SO_4)_2$ [b]	< 106	$NH_4Fe(SO_4)_2 \cdot 12\ H_2O$
NH_4MgPO_4 [b]	< 106	$NH_4MgPO_4 \cdot 6\ H_2O$
$AlNH_4(SO_4)_2$ [b]	< 106	$AlNH_4(SO_4)_2 \cdot 12\ H_2O$
$(NH_4)_3[Fe(C_2O_4)_3]$ [b]	< 106	$(NH_4)_3[Fe(C_2O_4)_3] \cdot 3\ H_2O$
Urea [b]	< 106	CH_4N_2O

The chemical composition of the de-agglomeration additives are summarized in Table 3Table 3, while the composition of the de-NO_X additives can be calculated from Table 2Table 2. Prior to combustion experiments, the additives were dry-mixed with the fuel using a rotational mixer. For the anti-agglomeration additives, approximately 4.7 g additive was added per 100 g of biomass based on the potassium capture capability of kaolin.[30,31] For the additives with NH-functionality, the theoretical NH_3/fuel-N molar ratio was kept at 1.5. It was assumed that the one mole of NH_4 or urea would produce one mole of NH_3.[32]

Table 3: Chemical composition of the additives. a: oxygen determined by calculation while remaining elements from ICP-OES [29], b: calculated from the chemical structure in Table 2Table 2. Crystalline water was not included in the calculations.

	wt% d.b.										
Additives	**O**	**Si**	**Al**	**Fe**	**Ca**	**Mg**	**Na**	**K**	**P**	**S**	**N**
Kaolin [a]	56.9	22.0	19.0	0.47	0.10	0.14	0.10	1.10	0.05	0.02	-
Coal fly ash [a]	46.6	22.0	14.0	2.90	4.50	0.97	0.27	0.87	0.64	0.26	-
Clay [a]	54.4	28.0	4.2	1.8	8.4	0.45	0.84	1.9	0.05	-	-
$MgCO_3$ [a]	50.3	-	-	-	-	41.1	-	-	-	-	-
CaO [a]	31.0	-	-	-	69.0	-	-	-	-	-	-

2.2 Thermogravimetric analyses (TGA) of additives

The decomposition of the de-NO_X additives was investigated in a thermogravimetric analyzeranalyzer (NETZSCH STA 449 F1), described in.[1] Approximately 2.5 mg of sample was heated from ambient temperature to 40 ºC and kept there for 20 min to remove moisture. A relatively low temperature was chosen employed to remove moisture to avoid thermal decomposition of the additives. Following this, the sample was heated at 5 ºC/min to 1100 ºC. All the additives were tested under inert conditions (50 NmL/min of N_2). Additionally, the influence of $(NH_4)_2SO_4$ particle size on the mass loss behaviourbehavior was investigated. Moreover, the influence of gas atmosphere on the decomposition of NH_4MgPO_4 and $AlNH_4(SO_4)_2$ was examined in inert and oxidizing (20% O_2) atmospheres, during which the gaseous decomposition products were characterized using mass spectrometry.

2.3 Continuous Fluidized bed Combustor

Figure 2Figure 2 depicts the bubbling fluidized bed reactor used for continuous combustion experiments, described in our previous work.[33] In all experiments, the concentrations of CO_2, CO, O_2, and NO in the flue gas was were measured using gas analyzers (NGA2000, Fischer-Rosemount). As the contribution of NO_2 to the total NO_X was less than 1%, this was not further considered.

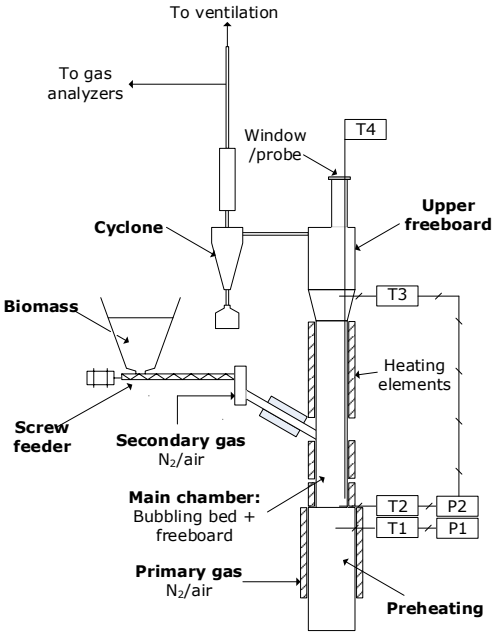

Figure 2: Schematic of the bubbling fluidized bed reactor. Adopted from [33].

For each test, 0.5 kg of silica sand was used, ensuring a static bed height of approximately 10 cm. The temperature in the bed was kept at 850ºC using external heating elements, and the excess air ratio (λ) was kept at 1.4 by varying the fuel feeding rate. Two different air staging configurations (λ_1/λ = 0.5 and 1) were examined for selected cases. In the case of straw-$(NH_4)_2SO_4$, the influence of additive particle size (<35 and <106 µm) and introduction method (batch addition or premixed with fuel) was ~~examined~~investigated. In the batch addition experiments, a single $(NH_4)_2SO_4$ pellet with a diameter, height, and weight of 10 mm, 3 mm, and 0.90 g, respectively, was added every 10 minutes. Continuous combustion experiments were performed until the point of defluidization or until all the prepared fuel was burned ~~out~~ off (0.3 kg for straw and 0.5 kg for sunflower husk). Complete defluidization was observed by either an increase (cake formation) or decrease (~~channelling~~channeling) in bed pressure. In addition, increasing localized temperature differences were observed prior to defluidization, as has been reported previously.~~.~~[34,35]~~.~~ Stable combustion was achieved in all cases, observed from the bed temperature measurements, and O_2 and CO_2 effluent concentrations. In one case (sunflower husk-$NH_4Al(SO_4)_2$), the ~~adhesion~~ adhesive forces of the additive~~s~~ led to pipe blockage and premature stop of the experiment.

The axial temperature profile in the reactor at steady state was measured by moving thermocouple T4 in Figure 2Figure 2. The measured temperature profiles were comparable between different combustion experiments, exemplified in the supplemental material (Figure S1-S3). This observation suggests that the employed additives had a negligible effect on the combustion behaviourbehavior of biomass. Consequently, the influence of temperature on the obtained results is expected to be small.

The concentration of gas at different heights in the reactor was determined using a water cooled probe inserted vertically from the top of the reactor. The sampled gas was sent to a Fourier Transform Infrared Spectrometer (FTIR) (Multigas 2030 FTIR, MKS instruments), from which the composition of various species such as NH_3, CO, NO, N_2O, CH_4 etc. was obtained. The repeatability of the straw-$(NH_4)_2SO_4$ combustion was reasonable, as demonstrated in the supplemental material (Figure S4).

3 Results and discussion

3.1 TGA of de-NOx additives

Figure 3Figure 3 summarizes the weight loss data from TGA of the de-NO_X additives. The decomposition onset temperature varied for the additives, from around 70 ºC for $(NH_4)_3[Fe(C_2O_4)_3]$ and $AlNH_4(SO_4)_2$ to around 250 ºC for $(NH_4)_2SO_4$. Several additives exhibited plateaus indicating the formation of solid decomposition byproducts. The observed mass loss behaviourbehavior is simplistically explained in Table 4Table 4 based on available literature. Notably, differences may be observed in the trends in the mass loss data and the information available in literature, due to the lumping of reactions (combination of dehydration etc.),, and differences in heating rate and gas atmosphere. Therefore, further studies are necessary to elucidate the decomposition mechanisms of some of the lesser known additives. The results show that all the additives release NH_3 and in all cases except for urea and $(NH_4)_2SO_4$, a residual solid was obtainedobserved. This residual could be P_4O_{10}, Fe_2O_3, $Mg_2P_2O_7$, or Al_2O_3.

Table 4: Simplified summary of the decomposition reactions of the additives.

Compound	Decomposition reactions and temperature
$(NH_4)_2SO_4$ [36]	$(NH_4)_2SO_4(s) \rightleftharpoons NH_4HSO_4(s) + NH_3(g)$ (250°C) $NH_4HSO_4(s) \rightleftharpoons NH_3(g) + H_2O(g) + SO_3(g)$ (390°C)
$(NH_4)_2HPO_4$ [37,38]	$(NH_4)_2HPO_4(s) \rightleftharpoons NH_4H_2PO_4(s) + NH_3(g)$ (< 170°C) $NH_4H_2PO_4(s) \rightleftharpoons H_3PO_4(s) + NH_3(g)$ (< 200°C) $4\ H_3PO_4(s) \rightleftharpoons P_4O_{10}(s) + 6\ H_2O(g)$ (> 200°C)
$(NH_4)_2Fe(SO_4)_2 \cdot 6\ H_2O$** [39]	$(NH_4)_2Fe(SO_4)_2 \cdot 6\ H_2O(s) \rightleftharpoons (NH_4)_2Fe(SO_4)_2(s) + 6\ H_2O(g)$ $(90 - 250°C)$ $2\ (NH_4)_2Fe(SO_4)_2(s) + \frac{1}{2}O_2(g) \rightleftharpoons Fe_2(SO_4)_3(s) + 4\ NH_3(g) + 2\ H_2O(g) + SO_3(g)$ $(250 - 350°C)^*$ $Fe_2(SO_4)_3(s) \rightleftharpoons Fe_2O_3(s) + SO_3(g) + 2\ SO_2 + O_2$ (> 350°C)*
$NH_4Fe(SO_4)_2 \cdot 12\ H_2O$ [39]	$NH_4Fe(SO_4)_2 \cdot 12\ H_2O(s) \rightleftharpoons NH_4Fe(SO_4)_2(s) + 12\ H_2O(g)$ (< 200°C) $2\ NH_4Fe(SO_4)_2 \rightleftharpoons Fe_2(SO_4)_3(s) + 2\ NH_3(g) + H_2O(g) + SO_3(g)$ $(250 - 350°C)^*$ $Fe_2(SO_4)_3(s) \rightleftharpoons Fe_2O_3(s) + SO_3(g) + 2\ SO_2 + O_2$ (> 350°C)*
Urea [40,41]	$CH_4N_2O(s) \rightleftharpoons NH_3(g) + HNCO(g)$ (> 152°C)

	Decomposition byproducts: biuret, cyanuric acid, and ammelide
$(NH_4)_3[Fe(C_2O_4)_3]\cdot 3$ H_2O [42]	$(NH_4)_3[Fe(C_2O_4)_3]\cdot 3\,H_2O(s) \rightleftharpoons (NH_4)_3[Fe(C_2O_4)_3](s) + 3\,H_2O(g) \quad (90-125°C)$
	$(NH_4)_3[Fe(C_2O_4)_3](s) \rightleftharpoons H_3Fe(C_2O_4)_3(s) + 3\,NH_3(g) \quad (190-235°C)$
	$2\,H_3Fe(C_2O_4)_3(s) \rightleftharpoons Fe_2O_3(s) + 3\,H_2O + 6\,CO + 6\,CO_2 \quad (245-275°C)^*$
$NH_4MgPO_4\cdot 6\,H_2O$ [43]	$NH_4MgPO_4\cdot 6\,H_2O\,(s) \rightleftharpoons MgHPO_4(s) + NH_3(g) + 6\,H_2O \quad (>55°C)$
	$2\,MgHPO_4(s) \rightleftharpoons Mg_2P_2O_7\,(s) + H_2O(g) \quad (1000°C)$
$AlNH_4(SO_4)_2\cdot 12\,H_2O$ [44]	$AlNH_4(SO_4)_2\cdot 12\,H_2O\,(s) \rightleftharpoons AlNH_4(SO_4)_2\,(s) + 12\,H_2O\,(g) \quad (30-230°C)^*$
	$2\,AlNH_4(SO_4)_2\,(s) \rightleftharpoons Al_2(SO_4)_3\,(s) + 2\,NH_3\,(g) + H_2SO_4\,(g) \quad (50-450°C)^*$
	$Al_2(SO_4)_3\,(s) \rightleftharpoons Al_2O_3(s) + 3\,SO_3(g) \quad (450-850°C)^*$

*Assumed global reactions based on literature data ** Oxidizing conditions

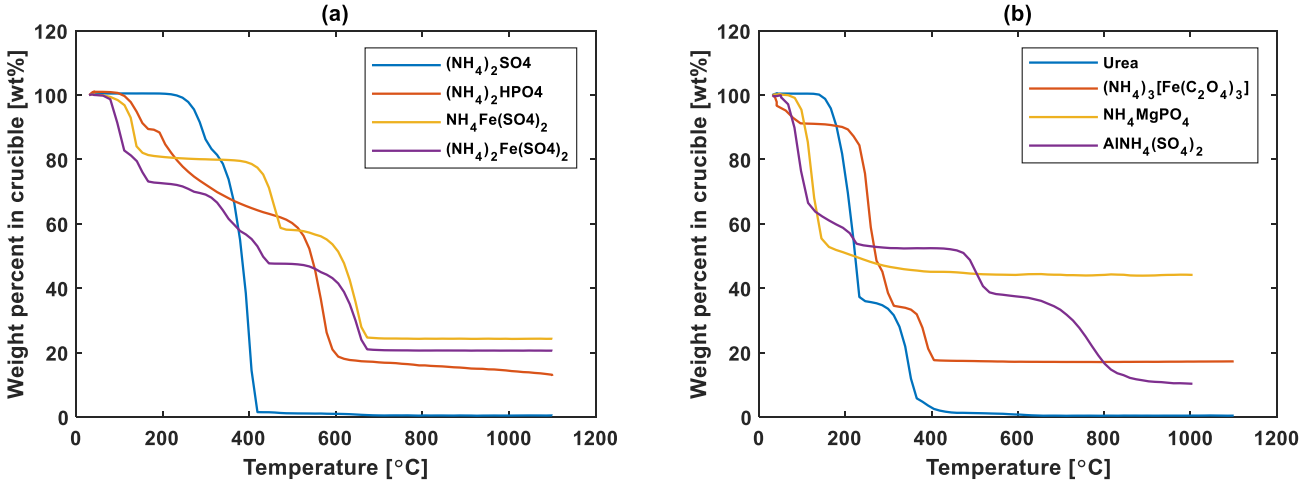

Figure 3: Weight loss data from TGA of de-NO_X additives in inert atmosphere.

TGA measurements were additionally conducted with varying atmosphere (inert and oxidizing) and $(NH_4)_2SO_4$ particle size (<35 µm and <105 µm) shown in the supplemental material (Figure S5). The results indicate that the examined parameters did not affect the weight loss ~~behaviour~~behavior significantly. In the case of NH_4MgPO_4 and $AlNH_4(SO_4)_2$, the decomposition products from TG experiments were ~~analysed~~analyzed by mass spectrometry, demonstrated in the supplemental material (Figure S6). These show that the nitrogen in the additives was predominantly released as NH_3 with and without the presence of air. In addition, some NO and N_2O was observed for $AlNH_4(SO_4)_2$ under oxidizing conditions due to the secondary oxidation of gases.

3.2 Straw-additive combustion

Figure 4Figure 4 shows the conversion of fuel-N to NO (a) and the defluidization tendency (b) during straw combustion with additives. For the anti-agglomeration additives, the results in Figure 4Figure 4a indicate that the fuel-N to NO conversion slightly increased when using CaO and $MgCO_3$, while coal fly ash, clay, and kaolin did not have a significant influence. CaO and possibly MgO have been suggested to increase NO emission in fluidized bed combustion by catalyzingcatalyzing the oxidation of NH_3 and HCN.[45,46] Of the NH-based containing additives, urea, $NH_4(SO_4)_2$, $AlNH_4(SO_4)_2$, and NH_4MgPO_4 decreased the fuel-N to NO conversion, while $(NH_4)_2HPO_4$, $(NH_4)_3[Fe(C_2O_4)_3]$, $(NH_4)_2Fe(SO_4)_2$, and $NH_4Fe(SO_4)_2$ had a negligible impact. The results show that the presence of an NH-functionality in the additives was necessary to reduce NO emission. In terms of defluidization tendency (Figure 4Figure 4b), kaolin, CaO, and $MgCO_3$ prevented defluidization, while coal fly ash and clay slightly prolonged the defluidization time. A deeper investigation of these is provided in [29], showing that kaolin captured fuel-K, preventing the formation of low melting K-silicates, whereas CaO and $MgCO_3$ increased the viscosity of the melt, thereby decreasing the propensity for agglomerate formation. Urea had a negligible impact on the defluidization behaviourbehavior, since the decomposition products of urea (HNCO and NH_3 [32]) are not expected to alter the ash chemistry significantly. For the multifunctional additives, defluidization was prevented by $(NH_4)_2Fe(SO_4)_2$, $NH_4Fe(SO_4)_2$, $AlNH_4(SO_4)_2$, and NH_4MgPO_4, prolonged by $NH_4(SO_4)_2$ and $(NH_4)_3[Fe(C_2O_4)_3]$, and accelerated by $(NH_4)_2HPO_4$. Generally, phosphates have been shown to decrease the defluidization tendency by forming crystalline K-Ca/Mg-phosphates; however, at a high concentration, low-temperature-melting phosphates may promote defluidization.[47–49] In the case of $(NH_4)_2HPO_4$, the formation of P_4O_{10}, which melts at 562°C, could have led to defluidization by sticking the bed material together.[37] The presence of S during combustion could convert the fuel-K to less harmful species such as K_2SO_4.[50] In addition, Al and Fe may increase the melting point of the compounds leading to agglomeration.[51] Of the examined additives, $AlNH_4(SO_4)_2$, and NH_4MgPO_4

were capable of reducing NO emission (approximately 40% reduction) while preventing defluidization.

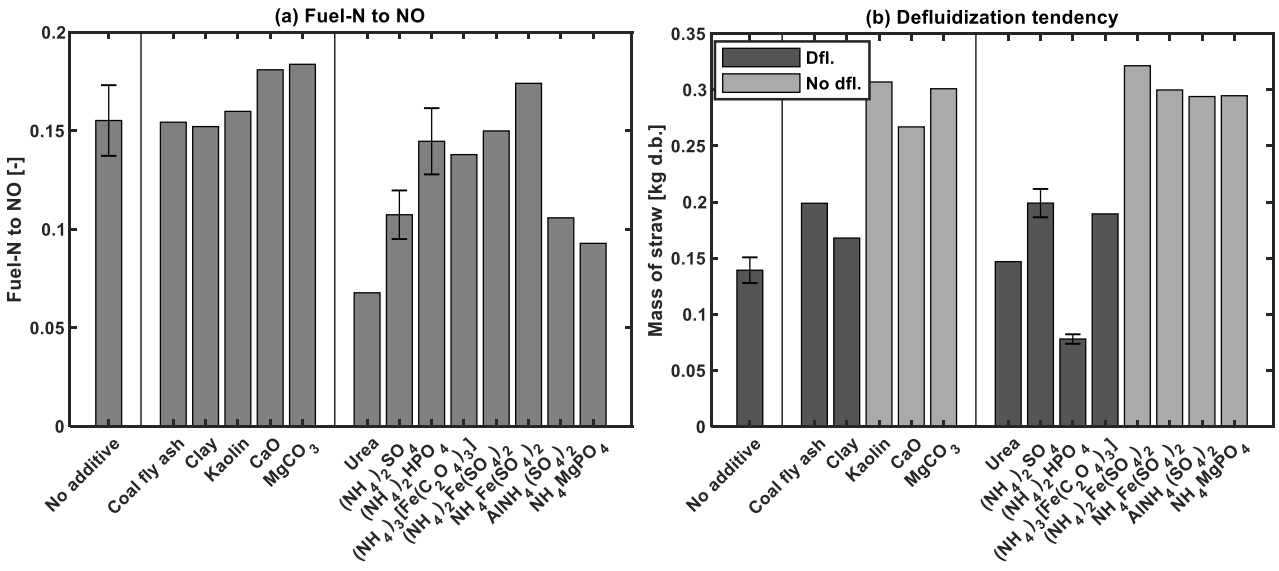

Figure 4: Fuel-N to NO conversion (a) and defluidization tendency, expressed in mass of straw combusted, (b) during straw combustion with additives. The fuel feeding rate (~0.110 kg d.b. straw/h) was constant and the mass of straw burned is proportional to the time before defluidization. Nomenclature: dlf: defluidization, no dfl: no defluidization. Conditions: T_{bed} = 850 ºC; λ = 1.4; λ_1/ λ = 1.

3.2.1 Local gas composition using de-NOx additives

Figure 5Figure 5a-f illustrates the NO, NH_3, and N_2O axial concentration profiles from during fluidized bed combustion of straw with additives. The plots on the left, i.e. Figure 5Figure 5a, c, and e, include the additives that led to a decrease in the fuel-N to NO conversion, while the plots on the right, i.e. Figure 5Figure 5b, d, and f, include the additives that had no significant influence on the fuel-N to NO conversion (cf. Figure 4Figure 4a). The concentration peaks indicate that the combustion reactions occurred predominantly between the sand bed and fuel inlet. In agreement with this, the CO and C_XH_Y profiles were comparable between experiments (supplemental material, Figure S7-S10), indicating that the differences observed in NO are predominantly related to the nitrogen chemistry, specifically NH_3. The NH_3 concentration in the reactor with additives was significantly higher than that of pure straw combustion, due to the decomposition of additives, which occurred predominantly above the fuel inlet and/or at the top of the fluid bed. While the outlet NO data of the Fe-based additives were comparable to that of raw straw, the local concentration measurements reveal a significantly

Form
Form
Form
Form

higher concentration of NO near the bed surface. This was caused by the catalytic effect of Fe on the oxidation of NH_3 to NO-.[46]. Moreover, the combustion with $(NH_4)_2HPO_4$ increased the NO emission near the bed compared to straw combustion. The reasoning for this was prescribed ascribed the poorer mixing as the bed approached defluidization, further explained in Section 3.4. Another explanation may be that the presence of P has had a direct or indirect[52] influence on the nitrogen chemistry (NH_3 oxidation and/or NO reduction), a topic which has received little attention in combustion research and would require further study. The results in Figure 5Figure 5 indicate that the additives, which did not substantially increase the NO concentration near the bed, were capable of reducing NO emission relative to pure straw combustion. This was caused by the facilitation of thermal $DeNO_X$ reactions due to a higher concentration of NH_3 in the reactor, i.e. R1 > R2.

$$NH_3 + NO + \frac{1}{4}O_2 \rightarrow N_2 + \frac{3}{2}H_2O \quad \text{R1}$$

$$NH_3 + \frac{5}{4}O_2 \rightarrow NO + \frac{3}{2}H_2O \quad \text{R2}$$

The results in Figure 5Figure 5e and f show that all the de-NO_X additives increased the N_2O concentration within the reactor. The highest N_2O emission was observed for urea, most likely due to the release and combustion of HNCO. The increased N_2O emission for the other additives was predominantly related to the larger concentration of NH_3 in the reactor, which may form N_2O by R3 and R4. Moreover, the presence of inorganic material such as Fe and Al may affect the selectivity for forming NO, N_2O, and N_2-.[46,53]. The relatively high concentrations of N_2O in this work could be a consequence of lower temperatures in the upper freeboard caused by the introduction of secondary gas, seen in the temperature profiles in the supplemental material (Figure S1-S3). As N_2O is strongly dependent on temperature-[54], this may be unimportant in industrial scale furnaces, in which freeboard temperatures can reach up to 1000 ºC-.[55].

$$NH_2 + NO_2 \rightarrow N_2O + H_2O \quad \text{R3}$$

$$NH + NO \rightarrow N_2O + H \quad \text{R4}$$

371

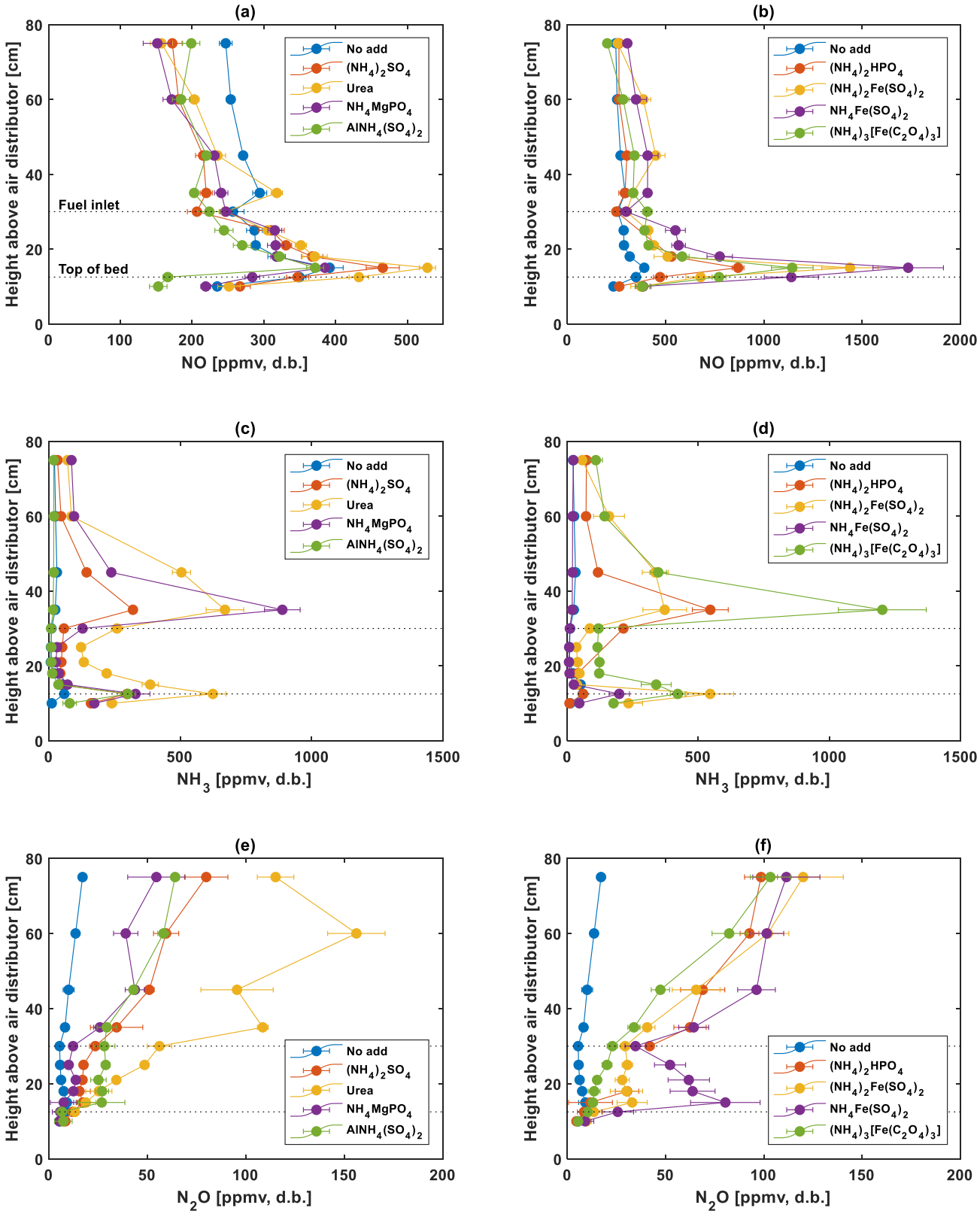

Figure 5: Axial NO (a,b), NH_3 (c,d), and N_2O (e,f) profiles during fluidized bed combustion of straw with different additives. For comparison the pure straw combustion profile is shown. The figures on the left (a,c,e) include the additives that led to a decrease in the fuel-N to NO conversion, while the figures on the right (b,d,f) include additives that did not alter fuel-N to NO conversion significantly (cf. Figure 4Figure 4a). The error bars indicate the temporal fluctuations in the measured concentrations. Conditions: T_{bed} = 850 °C; λ = 1.4; λ_1/λ = 1.

3.2.2 Influence of $(NH_4)_2SO_4$ particle size and introduction method

Figure 6Figure 6 depicts the local NO, NH_3, N_2O, and CO measurements during the combustion of straw with two different sizes of $(NH_4)_2SO_4$. The combustion behaviourbehavior was similar regardless of $(NH_4)_2SO_4$ particle size observed from the CO profile. Moreover, no significant difference was measured in the effluent concentrations of NO during combustion. However, slight differences are prominent from the local concentration data. For the smaller additive particle size range, more NH_3 was released above the fuel inlet, while for the larger range, NH_3 was released to a greater extent near the bed. The high NH_3 concentration above the fuel inlet led to a larger reduction of NO and higher concentration of N_2O for the smaller size range. In terms of defluidization tendency, complete defluidization was observed after combustion of 0.23 kg and 0.20±0.011 kg of straw for the $(NH_4)_2SO_4$ size ranges <106 µm and <35 µm, respectively. As the slight increase in mass of fuel burned for the larger particle sizes was higher than that of the standard deviation of several repetitions (±0.011 kg straw), the difference may be related to the larger proportion of additive reaching the bed. The concentrations of SO_2 and H_2SO_4 were similar in the reactor for the two additive size ranges, while a slightly higher SO_3 concentration was observed using the larger particle size range, seen in the supplemental material (Figure S11). However, the differences are small and caution must be taken as fluctuations in the feeding rate may affect the results.

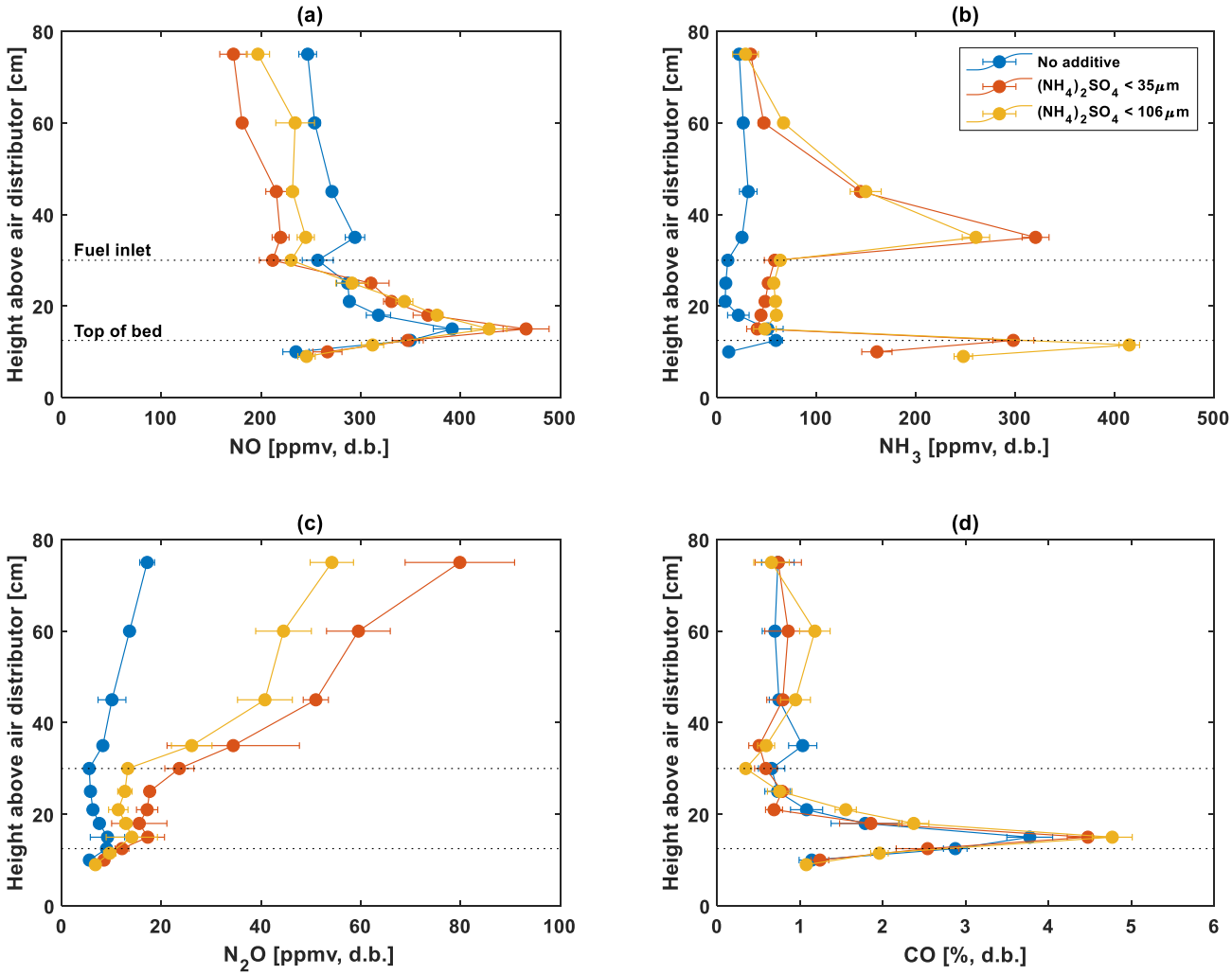

Figure 6: Axial NO (a), NH_3 (b), N_2O (c), and CO (d) profiles during fluidized bed combustion of straw with two different sizes of $(NH_4)_2SO_4$. Conditions: T_{bed} = 850 ºC; λ = 1.4; λ_1/λ = 1.

To investigate the influence of $(NH_4)_2SO_4$ addition method, $(NH_4)_2SO_4$ was either added as pellets during combustion or premixed with straw. The results are summarized in Table 5~~Table 5~~, showing that the fuel-N to NO conversion, average effluent CO concentration, and defluidization tendency were within the uncertainty determined from several repetitions. Consequently, no significant differences were observed from the two introduction methods. Based on the results in the previous paragraph, a larger particle size, in this case a pellet, would ensure that most of the $(NH_4)_2SO_4$ decomposed in the bed. Therefore, the amount of straw burned before defluidization would be expected to increase. The reason for the negligible difference between the two introduction methods may be related to distinct additive decomposition locations and/or mechanisms. The premixed smaller particles adhere to the fuel thereby achieving a closer contact with ash and gas components produced from combustion. In

Form

444 comparison, in the case of the pellet, the contact with the fuel and release mechanism differ, which
445 may lower the influence of the additive on the defluidization tendency. Further investigation would be
446 necessary to elucidate the mechanisms of the two addition methods. For both addition methods, a
447 reduction in fuel-N to NO conversion and increase in time before defluidization was observed relative
448 to straw combustion.

449 **Table 5:** The influence of $(NH_4)SO_4$ addition method on the fuel-N to NO, average CO concentration, and defluidization
450 tendency during straw combustion. For the premixed data, the $(NH_4)SO_4$ size was <35 µm.

Addition method	Fuel-N to NO [-]	Average CO [vol%, d.b.]	Defluidization tendency [kg straw d.b]
Batch (pellets)	0.0965	0.593	0.190
Premixed with straw	0.107 (± 0.0123)	0.801 (±0.261)	0.20 (± 0.011)

451

3.2.3 Influence of air staging

Figure 7Figure 7 describes the conversion of fuel-N to NO (a) and the defluidization tendency (b) during straw combustion with additives under different air staging configurations. The results show that air staging reduced the fuel-N to NO conversion by 40% during straw combustion. No synergy effect was observed during staged combustion with additives. On the contrary, a slightly higher fuel-N to NO conversion was observed during air staged combustion with $AlNH_4(SO_4)_2$. For both additives, no defluidization was observed during air staged and un-staged straw combustion.

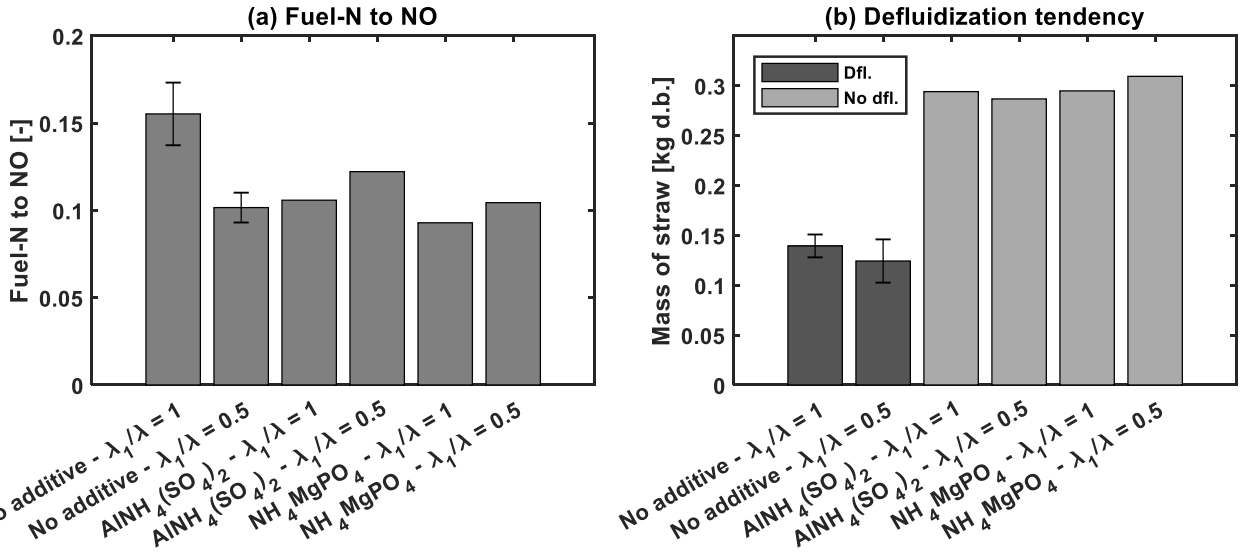

Figure 7: Fuel-N to NO conversion (a) and defluidization tendency, expressed in mass of straw combusted, (b) during straw combustion with additives with different staging configurations. Nomenclature: dlf: defluidization, no dfl: no defluidization. Conditions: T_{bed} = 850 ºC; λ = 1.4; λ_1/λ = 0.5 and 1.

Figure 8Figure 8 depicts the local concentration measurements during combustion of straw-NH_4MgPO_4 at air staged (λ_1/λ = 0.5) and un-staged (λ_1/λ = 1) conditions. The results show that during air staged combustion, the NO concentration was lower than the un-staged experiment below the secondary air injection point (fuel inlet). This was due to the facilitation of NO reducing reactions in a reducing atmosphere, indicated by the high CO concentration. Above the secondary air injection point, a comparable concentration of NH_3 was released to the freeboard. The fate of the NH_3 was determined by the mixing and O_2 concentration in the secondary jet. In air-staged combustion, the reduction of NO was less ~~favoured~~favored than in un-staged combustion. Consequently, the NO outlet concentration during air staged combustion with NH_4MgPO_4 surpassed the concentration from un-

staged combustion. A similar trend was additionally observed for the N_2O emission. The effluent CO concentration was higher in the air staged experiments, as the mixing and residence time in the reactor were inadequate for complete combustion. The results from straw-$AlNH_4(SO_4)_2$ combustion, illustrated in the supplemental material (Figure S12), exhibited a similar trend as in straw-(NH_4MgPO_4) combustion.

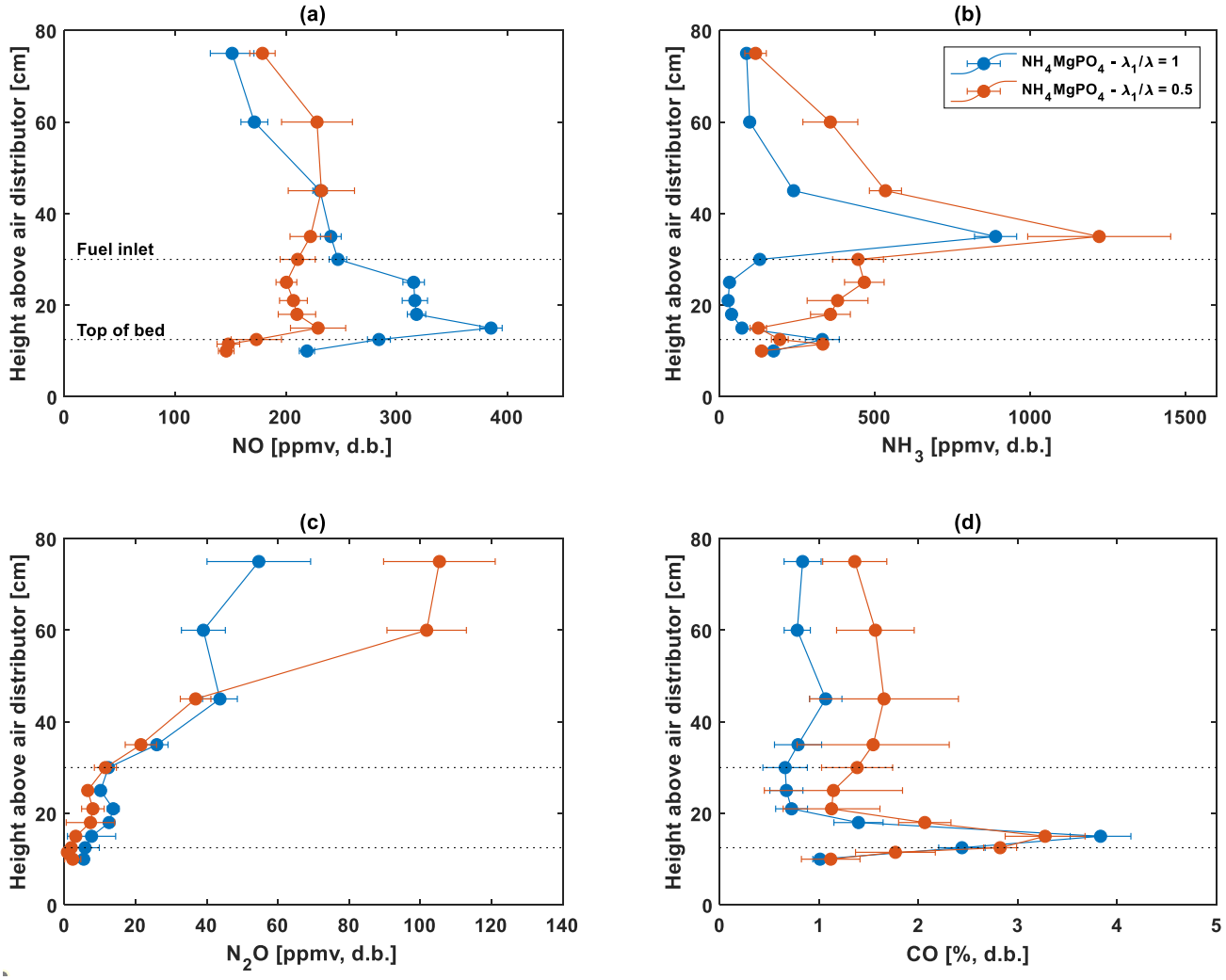

Figure 8: Axial NO (a), NH_3 (b), N_2O (c), and CO (d) profiles during fluidized bed combustion of straw-NH_4MgPO_4 under air staged and un-staged conditions. Conditions: T_{bed} = 850 ºC; λ = 1.4; λ_1/λ = 0.5 and 1.

3.3 Sunflower husk-additives combustion

Figure 9Figure 9 depicts the conversion of fuel-N to NO (a) and the defluidization tendency (b) during sunflower husk combustion with additives. The anti-agglomeration additives slightly increased the fuel-N to NO conversion, while the multifunctional additives reduced the fuel-N to NO conversion by 30%. Most additives prevented defluidization under the investigated conditions. In the case of $AlNH_4(SO_4)_2$, the experiment was stopped prematurely due to recurring blockage of the feeding pipe. However, it is suspected that $AlNH_4(SO_4)_2$ would prevent defluidization during sunflower husk combustion as well.

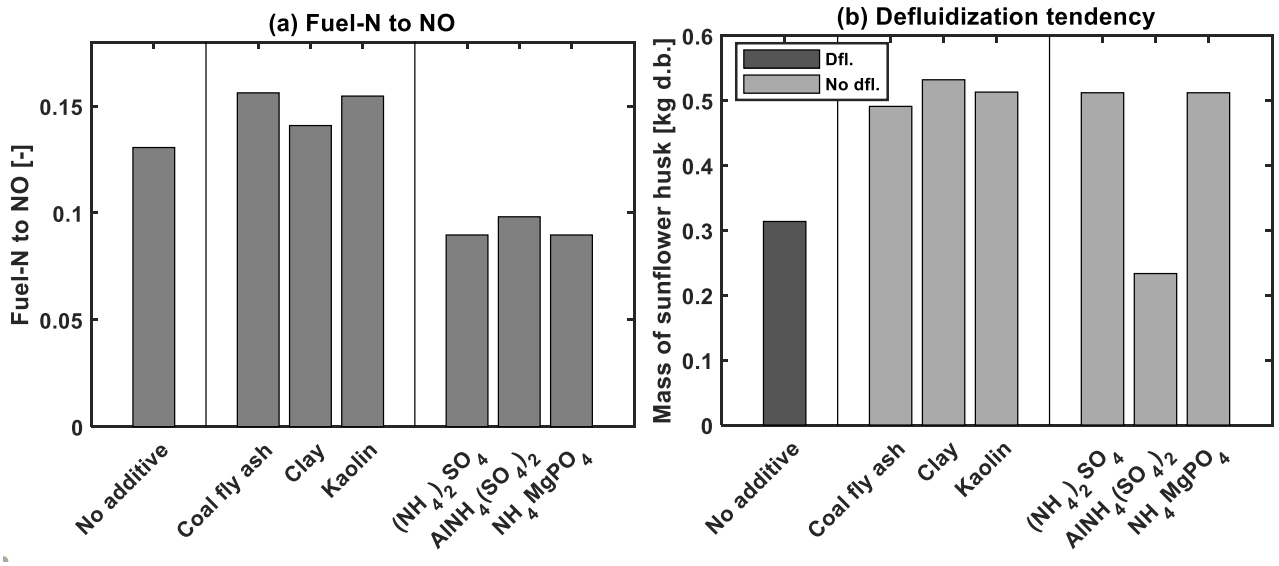

Figure 9: Fuel-N to NO conversion (a) and defluidization tendency, expressed in mass of sunflower husk combusted, (b) during sunflower husk combustion with additives. Experiment with $AlNH_4(SO_4)_2$ stopped prematurely due to feeding pipe blockage. Fuel feeding rate: (~0.110 kg d.b. sunflower husk/h). Nomenclature: dlf: defluidization, no dfl: no defluidization. Conditions: T_{bed} = 850 ºC; λ = 1.4; λ_1/λ = 1.

Figure 10Figure 10 illustrates the results of the local concentration measurements during combustion of sunflower husk with de-NO_X additives. The release location of NH_3 of the additives was similar to the experiments with straw, showing that NH_4MgPO_4 released a larger quantity of NH_3 above the fuel inlet, while $AlNH_4(SO_4)_2$ predominantly released NH_3 at the top of the bed. Consequently, the reduction of NO above the fuel inlet was more prominent for NH_4MgPO_4, while the NO concentration near the bed region was lower for $AlNH_4(SO_4)_2$. The CO profiles were comparable between experiments, indicating similar combustion ~~behaviour~~behavior of the fuels.

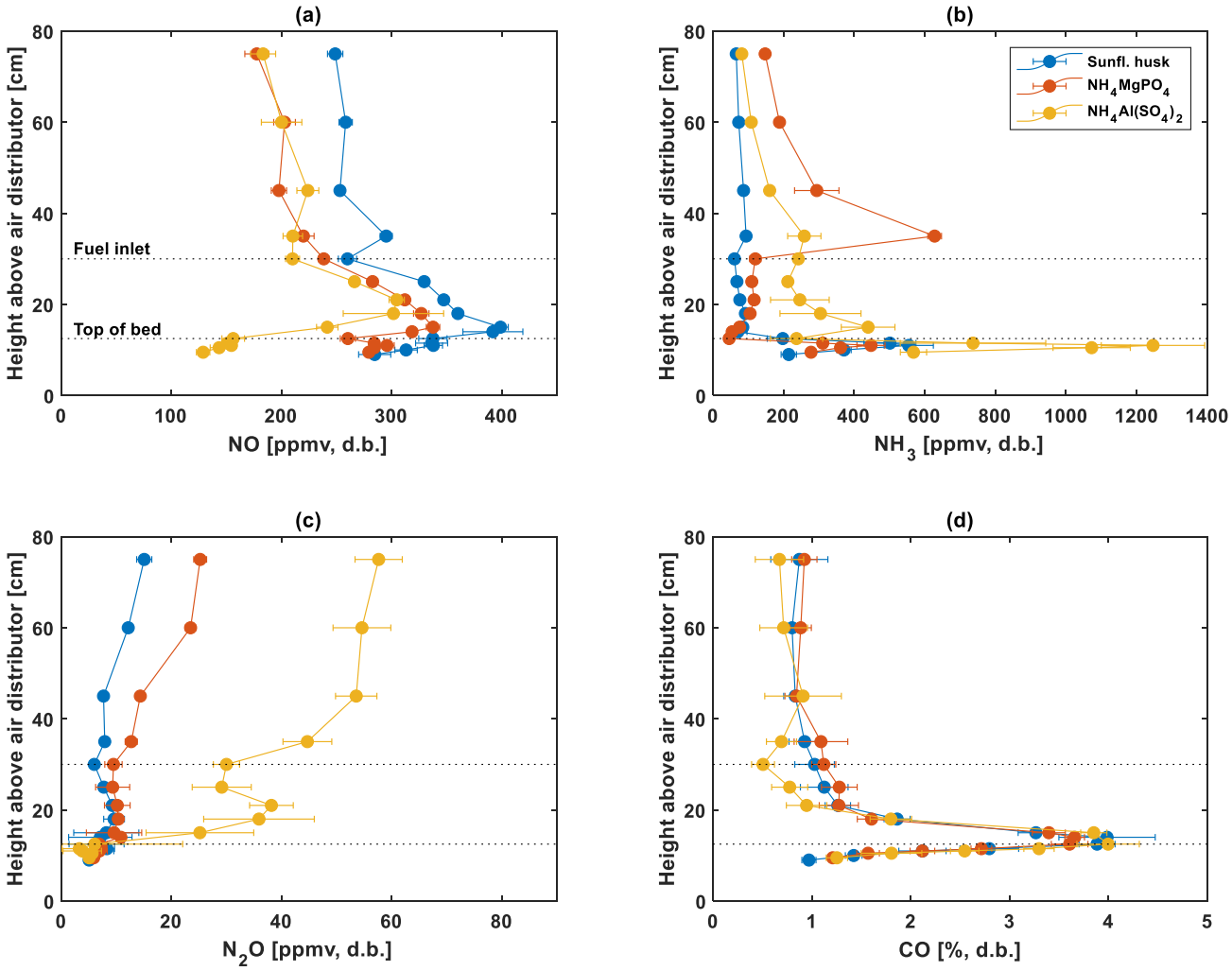

541

542 **Figure 10:** Axial NO (a), NH_3 (b), N_2O (c), and CO (d) profiles during fluidized bed combustion of sunflower husk with
543 NH_4MgPO_4 and $AlNH_4(SO_4)_2$. Conditions: T_{bed} = 850ºC; λ = 1.4; λ_1/ λ = 1.

3.4 Influence of defluidization on NOx emissions

The influence of ash accumulation and thereby bed agglomeration on the gaseous chemistry was investigated during pure sunflower husk combustion. Sunflower husk was chosen for this investigation, as it allowed local gas concentration measurements at the initial and late stages of combustion, since the time before defluidization was significantly longer than in straw combustion. The local concentration measurements are demonstrated in Figure 11Figure 11. The initial stage (init) measurements were conducted during the feeding of 0.04-0.15 kg d.b. sunflower husk (1.3-4.8 g ash), whereas the late stage (late) measurements were performed between 0.23-0.30 kg d.b. sunflower husk (7.4-9.6 g ash). While the overall trend in NO was similar, a slightly higher concentration of NO above the fuel bed was prominent at later stages of combustion. This was to some extent reflected in a slightly lower concentration of NH_3 at later stages of combustion. These differences may be attributed to the catalytic influence of ash on the light gas-N oxidation–[33,46] and/or to mixing limitations. Mixing limitations in the bed may be caused by the formation of a sticky molten layer on the bed particles leading to the formation of agglomerates. This molten phase changes the fluid dynamics and thereby the extent of fluidization during combustion, reflected in the slightly declining trend in bed pressure drop during combustion shown in the supplemental material (Figure S13). The worsening of the fluidization quality is additionally evident from the standard deviations of the concentration measurements near the top of the bed. In the early stages of combustion, larger temporal variations in the data (high standard deviation) were observed due to the burst of bubbles at the top of the bed. As the bed started to agglomerate and the fluid dynamics change, bubble bursting became less pronounced thereby dampening the temporal variation in the concentration measurements. Two mechanisms could explain the observed trends. Agglomerates formed during combustion could segregate and settle at the bottom of the bed–[34,56], thereby effectively minimizing the bed height and ultimately diminishing bubble size–.[57]. This could reduce the fluctuations caused by bubble bursting above the bed. Alternatively, viewing the sand bed as a continuous fluid, ash accumulation would increase the viscosity of the fluid, thereby slowly and continuously shifting the gas flow behaviourbehavior from

596 bubbling fluidization to plug flow, i.e. changing from complete mixing to plug flow
597 behaviourbehavior.[34]. A similar reasoning, i.e. poor mixing, may explain the increased NO emission
598 near the bed when employing $(NH_4)_2HPO_4$, described in Section 3.2.1. In addition, the accumulation
599 of sunflower husk ash had a negligible influence on the major C_XH_Y species, demonstrated the
600 supplemental material (Figure S14-S15).

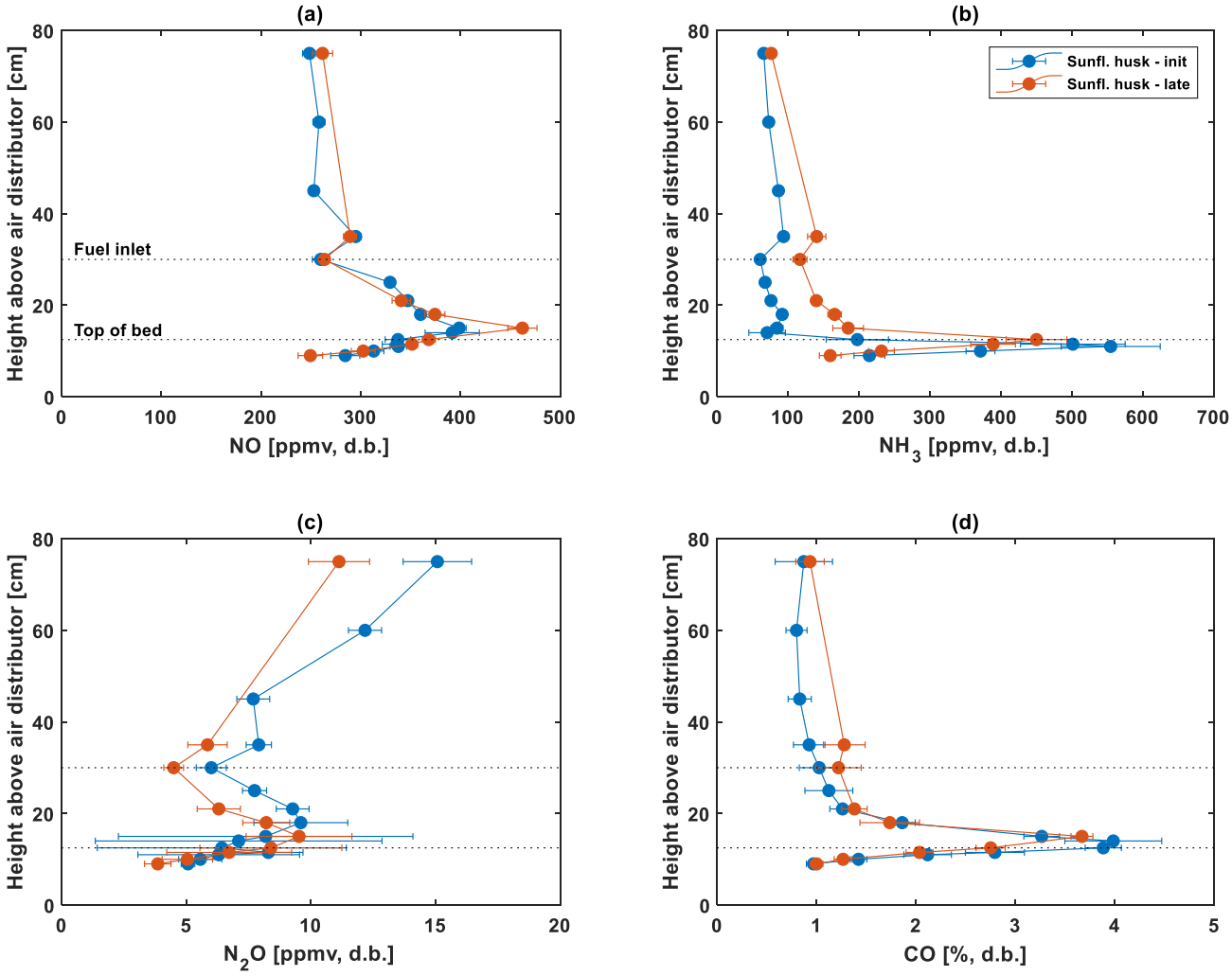

601

602 **Figure 11:** Axial NO (a), NH_3 (b), N_2O (c), and CO (d) profiles during fluidized bed combustion of sunflower husk.
603 Measurements were performed initial (init: 0.04-0.15 kg d.b. sunfl. husk) and late (init: 0.23-0.30 kg d.b. sunfl. husk) stages
604 of combustion. Conditions: T_{bed} = 850 ºC; λ = 1.4; λ_1/λ = 1.

4 Conclusions

The impact of a wide range of additives on NO_X emissions and bed agglomeration during continuous fluidized bed combustion of straw was investigated. The combustion ~~behaviour~~behavior of straw was unaffected by the presence of additives, notable from the local CO and C_XH_Y concentrations, and temperature measurements.

To reduce NO emission by additives, the release of NH_3 was necessary; however, not all NH_3 releasing additives ~~lead~~ led to a reduction in NO emission. Of the investigated additives, NH_4MgPO_4 and $AlNH_4(SO_4)_2$ prevented defluidization while reducing fuel-N to NO conversion by 40%. These additives were additionally effective during sunflower husk combustion, showing a 30% reduction in NO. The NH-based additives released NH_3 above the fuel inlet and/or bubbling bed. Some additives ~~favoured~~favored the reduction of NO by thermal $DeNO_X$ while others increased NO emission near the bed either due to the catalytic oxidation of NH_3 (Fe-based additives) or by inducing poor mixing conditions caused by the ash chemistry ($(NH_4)_2HPO_4$). All NH-based additives increased N_2O emission possibly by oxidation of NH_3. While NH_4MgPO_4 and $AlNH_4(SO_4)_2$ are promising additives, further work must be performed at variable experimental conditions (temperature, additive content, etc.) and the working mechanism should be elucidated.

The investigated $(NH_4)_2SO_4$ particle size ranges had a slight influence on the decomposition location, thereby affecting the local NO and N_2O concentrations. In comparison, the additive introduction method, i.e. batch wise as pellets or premixed with the fuel, had a negligible influence on NO emission and defluidization tendency.

Air staging reduced the fuel-N to NO conversion by 40% during straw combustion. The use of NH_4MgPO_4 and $AlNH_4(SO_4)_2$ under air staged conditions did not lead to a further decrease in NO; instead, the NO emission slightly increased when employing these additives with air staging. The introduction of secondary air ~~favoured~~favored the oxidation of NH_3 to NO to a larger degree than in un-staged combustion.

630 The accumulation of sunflower husk ash increased NO and decreased NH_3 concentration above
631 the bed, possibly caused by the incipient defluidization leading to poorer mixing and the catalytic
632 effect of ash forming elements on the nitrogen chemistry.
633

634 **Supporting information**

635 Information on axial reactor temperature profiles, repeatability, TGA data, local gas composition,
636 and bed pressure drop (PDF).
637

638 **Acknowledgements:**

639 This project is funded by the Sino-Danish Centre for Education and Research and Technical
640 University of Denmark.
641

642 **ToC graphic**

643 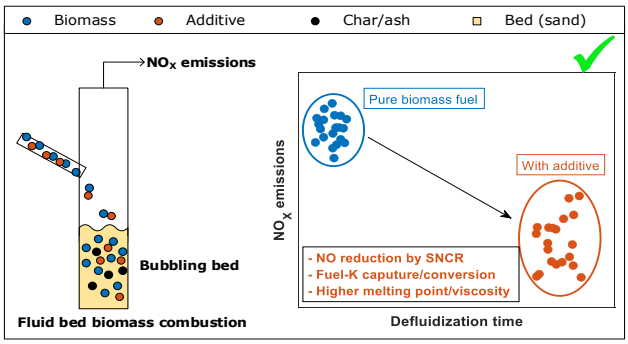

References

(1) Anicic, B.; Lin, W.; Dam-Johansen, K.; Wu, H. Agglomeration Mechanism in Biomass Fluidized Bed Combustion – Reaction between Potassium Carbonate and Silica Sand. *Fuel Process. Technol.* **2018**, *173* (October 2017), 182–190. https://doi.org/10.1016/j.fuproc.2017.10.005.

(2) Khan, A. A.; de Jong, W.; Jansens, P. J.; Spliethoff, H. Biomass Combustion in Fluidized Bed Boilers: Potential Problems and Remedies. *Fuel Process. Technol.* **2009**, *90* (1), 21–50. https://doi.org/10.1016/j.fuproc.2008.07.012.

(3) Leckner, B.; Karlsson, M. Gaseous Emissions from Circulating Fluidized Bed Combustion of Wood. *Biomass and Bioenergy* **1993**, *4* (5), 379–389.

(4) Werther, J.; Saenger, M.; Hartge, E. U.; Ogada, T.; Siagi, Z. Combustion of Agricultural Residues. *Prog. Energy Combust. Sci.* **2000**, *26* (1), 1–27. https://doi.org/10.1016/S0360-1285(99)00005-2.

(5) Chyang, C. S.; Qian, F. P.; Lin, Y.-C.; Yang, S.-H. NO and N2O Emission Characteristics from a Pilot Scale Vortexing Fluidized Bed Combustor Firing Different Fuels. *Energy and Fuels* **2008**, *22*, 1004–1011. https://doi.org/10.1016/j.fuel.2015.02.023.

(6) Hayhurst, A. N.; Vince, I. M. Nitric Oxide Formation from N2 in Flames: The Importance of "Prompt" NO. *Prog. Energy Combust. Sci.* **1980**, *6* (1), 35–51. https://doi.org/10.1016/0360-1285(80)90014-3.

(7) Hupa, M. Ash-Related Issues in Fluidized-Bed Combustion of Biomasses: Recent Research Highlights. *Energy and Fuels* **2012**, *26* (1), 4–14. https://doi.org/10.1021/ef201169k.

(8) Sher, F.; Pans, M. A.; Afilaka, D. T.; Sun, C.; Liu, H. Experimental Investigation of Woody and Non-Woody Biomass Combustion in a Bubbling Fluidised Bed Combustor Focusing on

Gaseous Emissions and Temperature Profiles. *Energy* **2017**, *141*, 2069–2080. https://doi.org/10.1016/j.energy.2017.11.118.

(9) Okasha, F. Staged Combustion of Rice Straw in a Fluidized Bed. *Exp. Therm. Fluid Sci.* **2007**, *32*, 52–59. https://doi.org/10.1016/j.expthermflusci.2007.01.006.

(10) Shimizu, T.; Tachiyama, Y.; Souma, M.; Inagaki, M. Emission Control of NOX and N2O of Bubbling Fluidized Bed Combustor. In *Proceedings of the International Conference on Fluidized Bed Combustion*; 1991; Vol. 2, pp 695–700.

(11) Gibbs, B. M.; Salam, T. F.; Sibtain, S. F.; Pragnell, R. J.; Gauld, D. W. The Reduction of NOx Emissions from a Fluidized Bed Combustor by Staged Combustion Combined with Ammonia Addition. *Twenty-Second Symp. Combust.* **1988**, 1147–1154. https://doi.org/10.1016/S0082-0784(89)80125-0.

(12) Dong, H.; Jiang, X.; Lv, G.; Wang, F.; Huang, Q.; Chi, Y.; Yan, J.; Yuan, W.; Chen, X.; Luo, W. Co-Combustion of Tannery Sludge in a Bench-Scale Fluidized-Bed Combustor: Gaseous Emissions and Cr Distribution and Speciation. *Energy and Fuels* **2017**, *31* (10), 11069–11077. https://doi.org/10.1021/acs.energyfuels.7b01831.

(13) Sirisomboon, K.; Kuprianov, V. I. Effects of Fuel Staging on the NO Emission Reduction during Biomass-Biomass Co-Combustion in a Fluidized-Bed Combustor. *Energy and Fuels* **2017**, *31* (1), 659–671. https://doi.org/10.1021/acs.energyfuels.6b02622.

(14) Kuprianov, V. I.; Ninduangdee, P.; Suheri, P. Co-Firing of Oil Palm Residues in a Fuel Staged Fluidized-Bed Combustor Using Mixtures of Alumina and Silica Sand as the Bed Material. *Appl. Therm. Eng.* **2018**, *144* (February), 371–382. https://doi.org/10.1016/j.applthermaleng.2018.08.089.

(15) de Diego, L. F.; de las Obras-Loscertales, M.; Rufas, A.; García-Labiano, F.; Gayán, P.; Abad,

690 A.; Adánez, J. Pollutant Emissions in a Bubbling Fluidized Bed Combustor Working in Oxy-
691 Fuel Operating Conditions: Effect of Flue Gas Recirculation. *Appl. Energy* **2013**, *102*, 860–867.
692 https://doi.org/10.1016/j.apenergy.2012.08.053.

693 (16) Abelha, P.; Gulyurtlu, I.; Cabrita, I. Release of Nitrogen Precursors from Coal and Biomass
694 Residues in a Bubbling Fluidized Bed. *Energy & Fuels* **2008**, *22* (1), 363–371.
695 https://doi.org/10.1021/ef700430t.

696 (17) Xu, G.; Ou, J.; Fang, B.; Wei, H.; Hu, T.; Wang, H. NOx Emission from the Combustion of
697 Mixed Fuel Pellets of Fenton/CaO-Conditioned Municipal Sludge and Rice Husk. *Environ.*
698 *Pollut.* **2021**, *281* (x), 117018. https://doi.org/10.1016/j.envpol.2021.117018.

699 (18) Kim, H. Y.; Baek, S. W.; Lee, C. Y. Effects of Hybrid Reburning System with SNCR and Air
700 Staging on NO x Reduction and Thermal Characteristics in Oxygen-Cnhanced Combustion.
701 *Combust. Sci. Technol.* **2009**, *181* (10), 1289–1309.
702 https://doi.org/10.1080/00102200903074246.

703 (19) Xu, H.; Smoot, L. D.; Hill, S. C. Computational Model for NOx Reduction by Advanced
704 Reburning. *Energy and Fuels* **1999**, *13* (2), 411–420. https://doi.org/10.1021/ef980090h.

705 (20) Chaivatamaset, P.; Tia, S. The Characteristics of Bed Agglomeration during Fl Uidized Bed
706 Combustion of Eucalyptus Bark. *Appl. Therm. Eng.* **2015**, *75*, 1134–1146.
707 https://doi.org/10.1016/j.applthermaleng.2014.10.046.

708 (21) Arromdee, P.; Kuprianov, V. I. Combustion of Peanut Shells in a Cone-Shaped Bubbling
709 Fluidized-Bed Combustor Using Alumina as the Bed Material. *Appl. Energy* **2012**, *97*, 470–
710 482. https://doi.org/10.1016/j.apenergy.2012.03.048.

711 (22) Öhman, M.; Nordin, A. The Role of Kaolin in Prevention of Bed Agglomeration during
712 Fluidized Bed Combustion of Biomass Fuels. *Energy & Fuels* **2000**, No. 14, 618–624.

https://doi.org/10.1021/ef990198c.

(23) Billen, P.; Costa, J.; Aa, L. Van Der; Westdorp, L.; Caneghem, J. Van; Vandecasteele, C. An Agglomeration Index for CaO Addition (as CaCO 3) to Prevent De Fl Uidization : Application to a Full-Scale Poultry Litter Fired FBC. *Energy & Fuels* **2014**, *28*, 5455–5462. https://doi.org/10.1021/ef500621w.

(24) Teixeira, P.; Lopes, H.; Gulyurtlu, I.; Lapa, N.; Abelha, P. Evaluation of Slagging and Fouling Tendency during Biomass Co-Firing with Coal in a Fluidized Bed. *Biomass and Bioenergy* **2012**, *39*, 192–203. https://doi.org/10.1016/j.biombioe.2012.01.010.

(25) Vamvuka, D.; Zografos, D.; Alevizos, G. Control Methods for Mitigating Biomass Ash-Related Problems in Fluidized Beds. *Bioresour. Technol.* **2008**, *99*, 3534–3544. https://doi.org/10.1016/j.biortech.2007.07.049.

(26) Bakker, R. R.; Jenkins, B. M.; Williams, R. B. Fluidized Bed Combustion of Leached Rice Straw. *Energy & Fuels* **2002**, *16* (2), 356–365. https://doi.org/10.1021/ef010197w.

(27) Maj, G.; Krzaczek, P.; Kuranc, A.; Piekarski, W. Energy Properties of Sunflower Seed Husk as Industrial Extrusion Residue. *Agric. Eng.* **2017**, *21* (1), 77–84. https://doi.org/10.1515/agriceng-2017-0008.

(28) Dodson, J. R.; Hunt, A. J.; Budarin, V. L.; Matharu, A. S.; Clark, J. H. The Chemical Value of Wheat Straw Combustion Residues. *RSC Adv.* **2011**, *1* (3), 523–530. https://doi.org/10.1039/c1ra00271f.

(29) Aničić, B. Agglomeration Mechanisms during Fluidized Bed Combustion of Biomass. Doctoral Thesis, Technical University of Denmark, 2018.

(30) Wang, G.; Jensen, P. A.; Wu, H.; Frandsen, F. J.; Sander, B.; Glarborg, P. Potassium Capture by Kaolin, Part 1: KOH. *Energy & Fuels* **2018**, *32*, 1851–1862.

https://doi.org/10.1021/acs.energyfuels.7b03645.

(31) Wang, G.; Jensen, P. A.; Wu, H.; Frandsen, F. J.; Sander, B.; Glarborg, P. Potassium Capture by Kaolin, Part 2: K2CO3, KCl, and K2SO4. *Energy and Fuels* **2018**, *32* (3), 3566–3578. https://doi.org/10.1021/acs.energyfuels.7b04055.

(32) Koebel, M.; Strutz, E. O. Thermal and Hydrolytic Decomposition of Urea for Automotive Selective Catalytic Reduction Systems: Thermochemical and Practical Aspects. *Ind. Eng. Chem. Res.* **2003**, *42* (10), 2093–2100. https://doi.org/10.1021/ie020950o.

(33) Ulusoy, B.; Anicic, B.; Lin, W.; Lu, B.; Wang, W.; Dam-Johansen, K.; Wu, H. Interactions in NOX Chemistry during Fluidized Bed Co-Combustion of Residual Biomass and Sewage Sludge. *Fuel* **2021**, *294* (X), 120431. https://doi.org/10.1016/j.fuel.2021.120431.

(34) Scala, F. Particle Agglomeration during Fluidized Bed Combustion: Mechanisms, Early Detection and Possible Countermeasures. *Fuel Process. Technol.* **2018**, *171* (July 2017), 31–38. https://doi.org/10.1016/j.fuproc.2017.11.001.

(35) Głód, K.; Lasek, J.; Słowik, K.; Zuwała, J.; Nabagło, D.; Jura, K.; Yrkowski, M. Investigation of Ash-Related Issues during Combustion of Maize Straw and Wood Biomass Blends in Lab-Scale Bubbling Fluidized Bed Reactor. *J. Energy Resour. Technol. Trans. ASME* **2020**, *142* (2), 1–11. https://doi.org/10.1115/1.4044221.

(36) Lv, X.; Cui, F.; Ning, Z.; Free, M. L.; Zhai, Y. Mechanism and Kinetics of Ammonium Sulfate Roasting of Boron-Bearing Iron Tailings for Enhanced Metal Extraction. *Processes* **2019**, *7* (11). https://doi.org/10.3390/pr7110812.

(37) Sevonius, C.; Yrjas, P.; Lindberg, D.; Hupa, L. Agglomeration Tendency of a Fluidized Bed during Addition of Different Phosphate Compounds. *Fuel* **2020**, *268* (January). https://doi.org/10.1016/j.fuel.2020.117300.

759 (38) Guerrant, G. O.; Brown, D. E. Thermal Decomposition of High-Analysis Fertilizers Based on
760 Ammonium Phosphate. *J. Agric. Food Chem.* **1965**, *13* (6), 493–497.
761 https://doi.org/10.1021/jf60142a002.

762 (39) Fekete, F.; Lázár, K.; Keszler, A. M.; Jánosity, A.; Zhibin, L.; Szilágyi, I. M.; Kótai, L.
763 Recycling the Industrial Waste ZnFe2O4 from Hot-Dip Galvanization Sludge. *J. Therm. Anal.*
764 *Calorim.* **2018**, *134* (3), 1863–1872. https://doi.org/10.1007/s10973-018-7849-8.

765 (40) Schaber, P. M.; Colson, J.; Higgins, S.; Thielen, D.; Anspach, B.; Brauer, J. Thermal
766 Decomposition (Pyrolysis) of Urea in an Open Reaction Vessel. *Thermochim. Acta* **2004**, *424*
767 (1–2), 131–142. https://doi.org/10.1016/j.tca.2004.05.018.

768 (41) Krum, K.; Patil, R.; Christensen, H.; Hashemi, H.; Wang, Z.; Li, S.; Glarborg, P.; Wu, H.
769 Kinetic Modeling of Urea Decomposition and Byproduct Formation. *Chem. Eng. Sci.* **2021**,
770 *230*, 116138. https://doi.org/10.1016/j.ces.2020.116138.

771 (42) Hussein, G. A. M.; Ismail, H. M.; Attyia, K. M. E. Physicochemical Investigation of the
772 Decomposition Products of Ammonium Metal Carboxylates: Ammonium Ferric Citrate
773 Hydrate. *J. Anal. Appl. Pyrolysis* **1995**, *31*, 157–167. https://doi.org/10.1016/0032-
774 5910(94)02860-5.

775 (43) Bhuiyan, M. I. H.; Mavinic, D. S.; Koch, F. A. Thermal Decomposition of Struvite and Its Phase
776 Transition. *Chemosphere* **2008**, *70* (8), 1347–1356.
777 https://doi.org/10.1016/j.chemosphere.2007.09.056.

778 (44) Kamruddin, M.; Ajikumar, P. K.; Dash, S.; Krishnan, R.; Tyagi, A. K.; Krishan, K. Non-
779 Isothermal Kinetics of Decomposition of A1NH4(SO4)2.12H2O by EGA-MS. *Thermochim.*
780 *Acta* **1996**, *287* (1), 13–23. https://doi.org/10.1016/0040-6031(96)02986-3.

781 (45) Shimizu, T.; Satoh, M.; Fujikawa, T.; Tonsho, M. Simultaneous Reduction of SO2 , NOX , and

782 N2O Emissions from a Two-Stage Bubbling Fluidized Bed Combustor. *Energy & Fuels* **2000**,
783 *14*, 862–868. https://doi.org/10.1021/ef9902202.

784 (46) Shimizu, T.; Toyono, M.; Ohsawa, H. Emissions of NO_X and N_2O during Co-Combustion of
785 Dried Sewage Sludge with Coal in a Bubbling Fluidized Bed Combustor. *Fuel* **2007**, *86*, 957–
786 964. https://doi.org/10.1016/j.fuel.2006.10.001.

787 (47) Grimm, A.; Skoglund, N.; Boström, D.; Boman, C.; Öhman, M. Influence of Phosphorus on
788 Alkali Distribution during Combustion of Logging Residues and Wheat Straw in a Bench-Scale
789 Fluidized Bed. *Energy and Fuels* **2012**, *26* (5), 3012–3023. https://doi.org/10.1021/ef300275e.

790 (48) Piotrowska, P.; Grimm, A.; Skoglund, N.; Boman, C.; Öhman, M.; Zevenhoven, M.; Boström,
791 D.; Hupa, M. Fluidized-Bed Combustion of Mixtures of Rapeseed Cake and Bark: The
792 Resulting Bed Agglomeration Characteristics. *Energy and Fuels* **2012**, *26* (4), 2028–2037.
793 https://doi.org/10.1021/ef300130e.

794 (49) Billen, P.; Creemers, B.; Costa, J.; Van Caneghem, J.; Vandecasteele, C. Coating and Melt
795 Induced Agglomeration in a Poultry Litter Fired Fluidized Bed Combustor. *Biomass and*
796 *Bioenergy* **2014**, *69*, 71–79. https://doi.org/10.1016/j.biombioe.2014.07.013.

797 (50) Wu, H.; Pedersen, M. N.; Jespersen, J. B.; Aho, M.; Roppo, J.; Frandsen, F. J.; Glarborg, P.
798 Modeling the Use of Sulfate Additives for Potassium Chloride Destruction in Biomass
799 Combustion. *Energy and Fuels* **2014**, *28* (1), 199–207. https://doi.org/10.1021/ef4015108.

800 (51) Olofsson, G.; Ye, Z.; Bjerle, I.; Andersson, A. Bed Agglomeration Problems in Fluidized-Bed
801 Biomass Combustion. *Ind. Eng. Chem. Res.* **2002**, *41* (12), 2888–2894.
802 https://doi.org/10.1021/ie010274a.

803 (52) Chang, S. G.; Lee, G. C. LBL PhoSNOX Process for Combined Removal of SO2 and NOX
804 from Flue Gas. *Environ. Prog.* **1992**, *11* (1), 66–73.

(53) Ninduangdee, P.; Kuprianov, V. I. Bioresource Technology Combustion of an Oil Palm Residue with Elevated Potassium Content in a Fluidized-Bed Combustor Using Alternative Bed Materials for Preventing Bed Agglomeration. *Bioresour. Technol.* **2015**, *182*, 272–281. https://doi.org/10.1016/j.biortech.2015.01.128.

(54) Glarborg, P.; Jensen, A. D.; Johnsson, J. E. Fuel Nitrogen Conversion in Solid Fuel Fired Systems. *Prog. Energy Combust. Sci. 29* **2003**, *29*, 89–113. https://doi.org/10.1016/S0360-1285(02)00031-X.

(55) Hupa, M.; Karlström, O.; Vainio, E. Biomass Combustion Technology Development - It Is All about Chemical Details. *Proc. Combust. Inst.* **2017**, *36* (1), 113–134. https://doi.org/10.1016/j.proci.2016.06.152.

(56) Balland, M.; Froment, K.; Ratel, G.; Valin, S.; Roussely, J.; Michel, R.; Poirier, J.; Kara, Y.; Galnares, A. Biomass Ash Fluidised-Bed Agglomeration: Hydrodynamic Investigations. *Waste and Biomass Valorization* **2017**, *8* (8), 2823–2841. https://doi.org/10.1007/s12649-017-9853-9.

(57) Rowe, P. N. Prediction of Bubble Size in a Gas Fluidised Bed. *Chem. Eng. Sci.* **1976**, *31* (4), 285–288. https://doi.org/10.1016/0009-2509(76)85073-7.